

## Identification of a RIP1 Kinase Inhibitor Clinical Candidate (GSK3145095) for the Treatment of Pancreatic Cancer

Philip A. Harris, Jill M. Marinis, John D Lich, Scott B. Berger, Anirudh Chirala, Julie A Cox, Patrick M Eidam, Joshua N. Finger, Peter J. Gough, Jae U Jeong, James Kang, Viera Kasparcova, Lara K Leister, Mukesh K. Mahajan, George Miller, Rakesh Nagilla, Michael T. Ouellette, Michael A. Reilly, Alan R. Rendina, Elizabeth J. Rivera, Helen H. Sun, James H. Thorpe, Rachel D Totoritis, Wei Wang, Dongling Wu, Daohua Zhang, John Bertin, and Robert W Marquis

ACS Med. Chem. Lett., **Just Accepted Manuscript** • DOI: 10.1021/acsmchemlett.9b00108 • Publication Date (Web): 09 May 2019

Downloaded from <http://pubs.acs.org> on May 10, 2019

### Just Accepted

“Just Accepted” manuscripts have been peer-reviewed and accepted for publication. They are posted online prior to technical editing, formatting for publication and author proofing. The American Chemical Society provides “Just Accepted” as a service to the research community to expedite the dissemination of scientific material as soon as possible after acceptance. “Just Accepted” manuscripts appear in full in PDF format accompanied by an HTML abstract. “Just Accepted” manuscripts have been fully peer reviewed, but should not be considered the official version of record. They are citable by the Digital Object Identifier (DOI®). “Just Accepted” is an optional service offered to authors. Therefore, the “Just Accepted” Web site may not include all articles that will be published in the journal. After a manuscript is technically edited and formatted, it will be removed from the “Just Accepted” Web site and published as an ASAP article. Note that technical editing may introduce minor changes to the manuscript text and/or graphics which could affect content, and all legal disclaimers and ethical guidelines that apply to the journal pertain. ACS cannot be held responsible for errors or consequences arising from the use of information contained in these “Just Accepted” manuscripts.



# Identification of a RIP1 Kinase Inhibitor Clinical Candidate (GSK3145095) for the Treatment of Pancreatic Cancer

Philip A. Harris,<sup>\*†</sup> Jill M. Marinis,<sup>†</sup> John D. Lich,<sup>†</sup> Scott B. Berger,<sup>†</sup> Anirudh Chirala,<sup>#</sup> Julie A. Cox,<sup>‡</sup> Patrick M. Eidam,<sup>†</sup> Joshua N. Finger,<sup>†</sup> Peter J. Gough,<sup>†</sup> Jae U. Jeong,<sup>†</sup> James Kang,<sup>†</sup> Viera Kasparcova,<sup>†</sup> Lara K. Leister,<sup>†</sup> Mukesh K. Mahajan,<sup>†</sup> George Miller,<sup>#§</sup> Rakesh Nagilla,<sup>†</sup> Michael T. Ouellette,<sup>‡</sup> Michael A. Reilly,<sup>†</sup> Alan R. Rendina,<sup>‡</sup> Elizabeth J. Rivera,<sup>†</sup> Helen H. Sun,<sup>†</sup> James H. Thorpe,<sup>§</sup> Rachel D. Totoritis,<sup>‡</sup> Wei Wang,<sup>#</sup> Dongling Wu,<sup>#</sup> Daohua Zhang,<sup>†</sup> John Bertin<sup>†</sup> and Robert W. Marquis<sup>†</sup>

<sup>†</sup>Pattern Recognition Receptor DPU and <sup>‡</sup> Medicinal Science & Technology, GlaxoSmithKline, Collegeville Road, Collegeville, Pennsylvania 19426, United States.

<sup>§</sup> Medicinal Science & Technology, GlaxoSmithKline, Gunnels Wood Road, Stevenage, Hertfordshire SG1 2NY, UK.

<sup>#</sup>S. Arthur Localio Laboratory, <sup>§</sup>Department of Cell Biology, New York University School of Medicine, 550 First Avenue, New York, NY 10016

**KEYWORDS** RIP1, type III kinase inhibitors, pancreatic cancer

**ABSTRACT:** RIP1 regulates cell death and inflammation and is believed to play an important role in contributing to a variety of human pathologies, including immune-mediated inflammatory diseases and cancer. While small-molecule inhibitors of RIP1 kinase have been advanced to the clinic for inflammatory diseases and CNS indications, RIP1 inhibitors for oncology indications have yet to be described. Herein we report on the discovery and profile of GSK3145095 (compound **6**). Compound **6** potently binds to RIP1 with exquisite kinase specificity and has excellent activity in blocking RIP1 kinase-dependent cellular responses. Highlighting its potential as a novel cancer therapy, the inhibitor was also able to promote a tumor suppressive T cell phenotype in pancreatic adenocarcinoma organ cultures. Compound **6** is currently in phase 1 clinical studies for pancreatic adenocarcinoma and other selected solid tumors.

Receptor interacting proteins (RIP) 1 and 3 are known to form a complex termed the necrosome that leads to a form of cell death called necroptosis and inflammatory cytokine production.<sup>1</sup> Necroptosis can drive an inflammatory response through release of damage-associated molecular patterns<sup>1</sup> and the necrosome is also thought to contribute to neuronal cell loss in neurodegenerative diseases.<sup>2</sup> Several RIP1 inhibitors are now progressing in the clinic for the treatment of inflammatory diseases, such as psoriasis, rheumatoid arthritis and ulcerative colitis,<sup>3</sup> as well for CNS indications such as ALS and Alzheimer's disease.<sup>2</sup> Additional functions of the RIP1 continue to be discovered. Recently Seifert and Miller have reported that the necrosome can also promote an immune suppression in pancreatic tumors.<sup>4</sup> Additionally, Miller's lab, in collaboration with our group, have shown that RIP1 kinase inhibition resulted in T cell differentiation towards a tumor suppressive phenotype leading to tumor-immunity in mice and in models of human pancreatic cancer.<sup>5</sup> Importantly, RIP1 kinase inhibition sensitized tumors to checkpoint blockade, offering the potential for

combination with PD-1 immunotherapy as a new option for the treatment of pancreatic cancer. We report in this Letter on the identification of a new clinical RIP1 inhibitor for pancreatic cancer and other solid tumors.

The first reported RIP1 inhibitors discovered by Degterev et al., exemplified by indole-hydantoin **1** (see Figure 1), were shown by co-crystallized in the RIP1 kinase domain to occupy an allosteric lipophilic pocket at the back of the ATP binding site.<sup>6,7</sup> This type III binding mode, resulted in an excellent kinase selectivity profile.<sup>8</sup> Our screening efforts against DNA-encoded libraries led to the identification of a benzoxazinone RIP1 inhibitor **2** (GSK'481), whose RIP1 co-crystal structure showed it occupied the same allosteric binding pocket as **1**.<sup>9</sup> Subsequent lead-optimization resulted in selection of development candidate **3** (GSK2982772), which is currently under evaluation in phase 2a clinical trials in psoriasis, rheumatoid arthritis and ulcerative colitis patients.<sup>10</sup> Recently, Yoshikawa et al. have disclosed a benzoxazinone analog **4** with a higher brain penetration and efficacy in a

mouse experimental autoimmune encephalomyelitis (EAE) model of multiple sclerosis.<sup>11</sup>

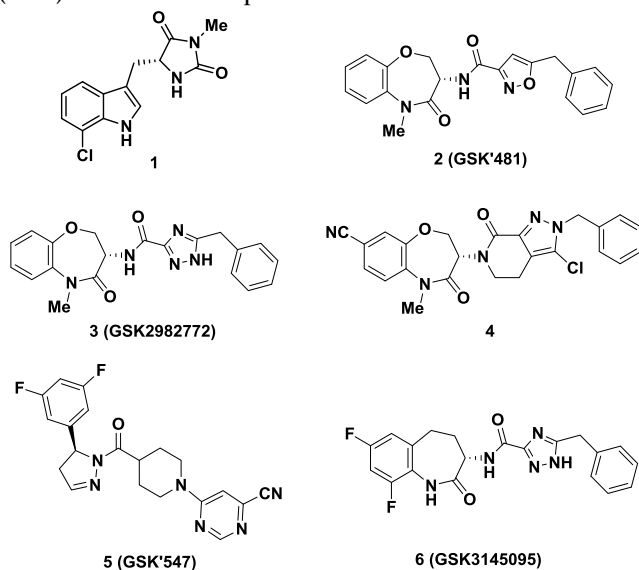


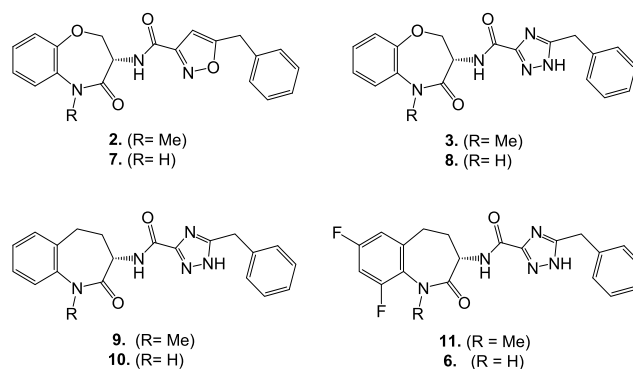
**Figure 1.** Structure of RIP1 kinase inhibitors.

We recently disclosed the efficacy of RIP1 inhibitor **5** (known as GSK'547) in an oncology mouse model of pancreatic cancer in both reducing tumor size and activating an immune cell response.<sup>5</sup> Co-treatment of **5** with either a PD-1 antibody, to block immune down-regulation, or an ICOS antibody, to stimulate immune signalling, further reduced tumor size. Although **5** was an excellent tool for exploring RIP1 inhibition in mouse oncology models, it did not possess the required preclinical profile to support development as a clinical lead, most notable suffering from high turnover in human hepatocytes. Herein we describe the identification of a new RIP1 inhibitor clinical candidate (S)-5-benzyl-N-(7,9-difluoro-2-oxo-2,3,4,5-tetrahydro-1H-benzo[b]azepin-3-yl)-1H-1,2,4-triazole-3-carboxamide **6** (GSK3145095), structurally related to benzoxazepinone **3**. Although **3** is in clinical development for chronic immunoinflammatory disorders, development of a separate RIP1 inhibitor for oncology indications with their distinct safety tolerance and dosing criteria was required. The high RIP1 potency, mono-kinase selectivity and excellent preclinical pharmacokinetic and developability profile of benzazepinone **6** led to its selection for clinical development and it recently initiated phase 1 evaluation in pancreatic cancer patients.

We have recently detailed the lead optimization of the DNA-encoded library derived hit benzoxazepinone **2** that led to identification of **3**, the first RIP1 inhibitor to enter clinical evaluation.<sup>10</sup> Since the SAR observations identified during the discovery of benzoxazepinone **3** also apply to benzazepinone **6** only a brief synopsis of some of the key modifications is warranted here. As a benchmark, benzoxazepinone **2** possessed excellent RIP1 in vitro potency, as measured by both an ADP-Glo biochemical

assay and a human monocytic U937 cellular assay, but suffered from high lipophilicity and suboptimal pharmacokinetic (PK) profile (Table 1).<sup>9</sup> The corresponding NH lactam analog **7** possessed a better rat PK profile but at the cost of lower RIP1 potency. This was a general trend observed in this series: methylation of the amide increased RIP1 potency by up to 10-fold, as the methyl group occupies a small pocket on the face of the  $\beta$ -sheet defined by Leu90-Met92 and Ile43-Lys45.<sup>10</sup> However, metabolic demethylation of the N-methyl lactam can increase turnover, thus NH lactams tended to have better in vivo exposures. Replacement of the isoxazole of both **2** and **7** with a triazole (analogs **3** and **8**) maintained comparable RIP1 potencies with significantly reduced lipophilicity and improved rat oral exposures. Replacement of the benzoxazepinone heterocycle for benzazepinone **9** and **10** showed comparable in vitro potencies. Finally, introduction of 7,9-difluoro substitution at the benzazepinone yielded analogs **11** and **6**. The increase in potency of **6** compared to **10** could be attributed to the two electron withdrawing fluorines decreasing the pKa of the lactam nitrogen, thus strengthening its H-bond to the backbone of Leu90 (Figure 2). The NH-lactam of **6** predictably increased rat exposure compared to NMe-lactam **11**. The optimal potency and rat oral PK profile of benzazepinone **6** led to further pre-clinical evaluation as detailed below.

**Table 1.** SAR summary of key compounds



Cpd	ADP-Glo <sup>a</sup> IC <sub>50</sub> (nM)	U937 <sup>a</sup> IC <sub>50</sub> (nM)	CHI log D <sup>b</sup>	Rat AUC <sub>0-∞</sub> <sup>c</sup> μg.h/mL
<b>2</b>	1.6	7.9	5.9	0.38
<b>7</b>	32	200	5.1	2.2
<b>3</b>	1.0	6.3	3.8	2.3
<b>8</b>	32	100	3.0	2.5
<b>9</b>	5.0	10	3.8	0.31
<b>10</b>	50	63	3.1	nd
<b>11</b>	6.3	6.3	4.3	0.16
<b>6</b>	6.3	10	3.4	1.1

<sup>a</sup>Assay protocols are described in Supporting Information; IC<sub>50</sub> values are the average of at least two determinations. <sup>b</sup>CHI

(chromatographic hydrophobicity index)  $\log D$  at pH 7.4 was calculated from the retention time ( $t_R$ ) observed in a fast gradient reverse-phase HPLC. <sup>c</sup>Rat oral exposure at 2 mg/kg.

Co-crystallization of benzazepinone **6** was achieved with the RIP1 construct (1–294, C34A, C127A, C233A, and C240A). The resulting X-ray structure was refined to resolution of 2.87Å (see Supporting Information). In this structure, benzazepinone **6** was observed to be buried deep in the pocket between the N-terminal and C-terminal domains with no interaction with the hinge residues, making this a type III class of kinase inhibitor (see Figure 2). The triazole and benzyl functionality of **6** occupies the same allosteric lipophilic pocket at the back of the ATP binding site as Necrostatin-4. The benzoxazepine ring occupies space where the  $\alpha$ -phosphate of ATP would reside, so the inhibition is not strictly allosteric. The amide carbonyl attached to the triazole makes a direct hydrogen bond interaction with the backbone amide NH of Asp156. The triazole nitrogen makes a water mediated hydrogen bond to the carbonyl oxygen of Met67. The lactam nitrogen shows a possible long hydrogen bond interaction to the backbone carbonyl of Leu90 and the fluorine at the 9-position of the benzazepinone occupies a pocket between Met92 and Ile43. Details on co-crystallography are available in the Supporting Information section.

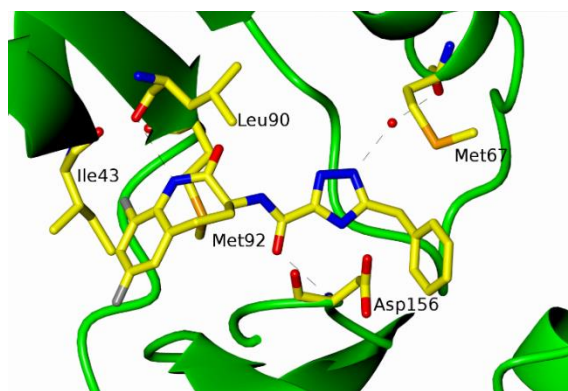


**Figure 2.** Co-crystal structure of RIP1 (1–294, C34A, C127A, C233A, and C240A) and benzazepinone **6**.

The type III binding mode observed for this pharmacophore in RIP1 results in complete kinase selectivity for RIP1 as exemplified by the kinase profile of **6** against both a P33 radiolabeled assay screen at Reaction Biology Corp (359 kinases) and a competition binding assay KINOMEScan at DiscoverX Corp (456 kinases). In both assays benzazepinone **6** was tested at a concentration of 10  $\mu$ M and showed no inhibition of any kinase other than RIP1, representing a >1500-fold selectivity window based on the RIP1 ADP-Glo potency of 6.3 nM. Details are available in the Supporting Information section.

Although benzazepinone **6** is binding in an allosteric pocket at the back of the ATP binding site, it is also partially occupying the region where the  $\alpha$ -phosphate of ATP

would reside, making them mutually exclusive, and ATP competitive inhibition is indeed observed (see Supporting Information). The binding kinetics are similar to benzoxazepinones recently profiled, with a moderate on-rate constant ( $k_{on} = 2.5 \times 10^4 \text{ M}^{-1}\text{s}^{-1}$ ), accompanied by a slow off-rate constant  $k_{off} = 1.2 \times 10^{-4} \text{ s}^{-1}$  ( $t_{1/2} = 99 \text{ min}$ ), measured by stopped-flow kinetics and fluorescence polarization competitive binding, respectively (see Supporting Information). In addition to efficacy against the immortalized U937 human monocyte cell line, activity of **6** was also assessed in primary neutrophils isolated from human whole blood. As previously described, in this assay TNF is co-incubated with both the caspase inhibitor QVD-Oph and the SMAC mimetic RMT 5265, which block the apoptosis and NF- $\kappa$ B pathways, respectively, driving the TNF response down the necrosis pathway.<sup>10</sup> Inhibitor **6** was able to potently block this response as shown by determination of overall cell viability as measured by cellular ATP levels ( $IC_{50} = 1.6 \text{ nM}$ ), cell death as measured by LDH release ( $IC_{50} = 0.5 \text{ nM}$ ) and RIP1-dependent inflammatory cytokine MIP-1 $\beta$  production, either as absolute levels for protein, or fold changes in mRNA expression ( $IC_{50} = 0.4 \text{ nM}$ ).

A human whole blood stimulation assay was previously developed in which the necroptosis pathway is activated through stimulation with TNF co-incubated with the caspase inhibitor QVD-Oph or zVAD.fmk, and the SMAC mimetic RMT 5265.<sup>10</sup> In this assay benzazepinone **6** was also shown to be very potent as measured by inhibition of cytokine MIP-1 $\beta$  ( $IC_{50} = 5 \text{ nM}$ ). In a similar monkey whole blood stimulation assay, benzazepinone **6** exhibited an  $IC_{50}$  of 16 nM.

A distinctive feature of RIP1 type III inhibitors is a significant reduction in potency against non-primate RIP1.<sup>9</sup> Compound **6** is over 380-fold less potent against non-primate RIP1 compared to primate RIP1 in biochemical assays (see Supporting Information) and shows a 340-fold reduction in cellular potency for blockage of necrotic death in mouse fibrosarcoma L929 cells ( $IC_{50} = 1.3 \mu\text{M}$ ) compared to human U937 cells ( $IC_{50} = 6.3 \text{ nM}$ ). This reduced RIP1 mouse potency precludes evaluation of **6** in rodent oncology models. However, **6** was evaluated in human *ex vivo* tumor cultures. For these studies, patient derived organotypic spheroids (PDOTS) were prepared from freshly resected tumors from pancreatic adenocarcinoma, colorectal, breast and gastric cancer patients, as previously described.<sup>12</sup> PDOTS were treated with **6** or vehicle and following 3 days incubation, they were harvested and analysed by flow cytometry (see Figure 3). PDOTS treated with **6** developed significantly more effector-memory T cells (CD44+) and immunogenic CD4+ T cells (IFN $\gamma$ +) compared to vehicle treated samples. A trend toward increase CD8+ cytolytic T cells and TNF $\alpha$  expression was also observed (see Supporting

Information); however, those markers failed to reach statistical significance in this study. Patients with increased T-cell infiltration and activation have a better prognosis with longer survival and response to immunotherapy agents.<sup>13</sup> This agrees with earlier results in the orthotopic mouse model of pancreatic cancer where RIP1 inhibition leads to an immunogenic tumor microenvironment.<sup>5</sup>

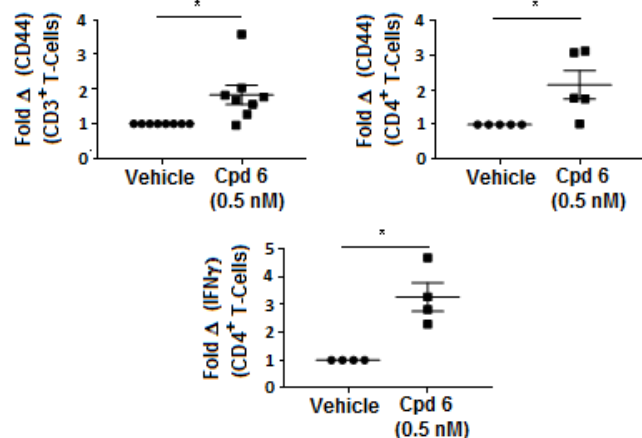


**Figure 3.** Individual PDOTs were prepared from resected patient tumors and incubated for 3 days with vehicle or compound **6** (0.5 nM in culture medium). Cells were labeled with antibodies to detect CD3 (pan-T cells), CD4 (T helper cells), CD44 (effector-memory cells), and IFN $\gamma$  (marker of T cell activation) then analyzed by flow cytometry. The percentage of cells expressing the indicated marker in vehicle treated samples was set to 1 and the fold change in the presence of compound **6** determined.

Benzazepinone **6** displayed a good free fraction in blood of rat (13%), dog (12%), monkey (12%) and human (8.1%). In vitro evaluation of the metabolic stability of **6** in hepatocytes indicated moderate turnover in the rat and low turnover in monkey and human (see Supporting Information). A metabolite identification study in rat, monkey and human hepatocytes highlighted that **6** was metabolized via both phase I and phase II biotransformation pathways, as shown in Figure 4. The primary metabolic pathways for **6** included hydroxylation and glucuronidation. No human specific metabolites of **6** were detected in these hepatocyte incubations, but trace levels of GSH conjugates were detected only in rat and monkey, not in human hepatocyte incubations. A pharmacokinetic evaluation of **6** in rat, dog and monkey demonstrated a low clearance ( $\leq 35\%$  liver blood flow) in all species (see Table 2). The volume of distribution was moderate along with a relatively short to moderate terminal half-life. Good oral bioavailability was observed across these preclinical species. The tissue distribution of **6** in rat was evaluated following iv infusion over 4 hours (see Supporting Information). This study showed that compared to blood **6** distributed at greater concentrations (7-8 fold) in liver and

kidney, and comparable concentrations (0.7-3 fold) in colon, heart and skin. In contrast, **6** had low brain penetration (6%) despite possessing moderate cell permeability ( $6.7 \times 10^{-6}$  cm/s), which is likely due to active extrusion from brain via the efflux drug transporter P-glycoprotein (P-gp) (see Supporting Information).

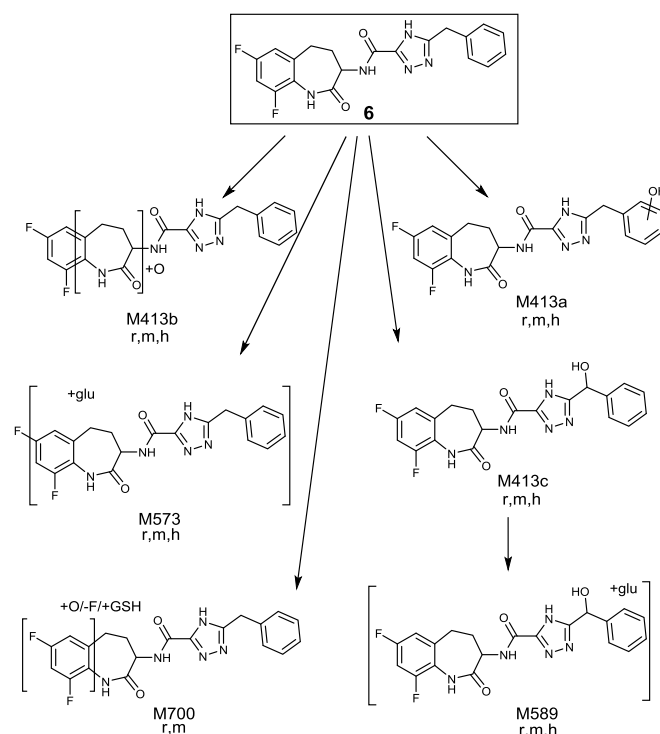


**Figure 4.** Proposed metabolic pathways of compound **6** in rat (r), monkey (m) and human (h) hepatocytes.

**Table 2. Pharmacokinetic Parameters of **6** Following Administration to Rat, Dog and Monkey**

Route	Parameter	Rat	Dog	Monkey
iv <sup>a</sup>	dose (mg/kg)	1.0	1.1	0.93
	Cl (mL/min/kg) (%LBF)	27 ± 5 (35)	9.8 ± 1.8 (18)	6.4 ± 0.5 (15)
	Vdss (L/kg)	1.8 ± 0.3	1.1 ± 0.2	1.8 ± 0.1
	t <sub>1/2</sub> (h)	2.2 ± 0.8	1.7 ± 0.02	4.2 ± 0.6
po <sup>b</sup>	dose (mg/kg)	2.1	2.0	1.9
	T <sub>max</sub> (h)	0.83 ± 0.29	0.75 ± 0.43	1.5 ± 0.0
	C <sub>max</sub> (μg/mL)	320 ± 79	910 ± 130	770 ± 99
	AUC (μg·h/mL)	1.1 ± 0.2	2.5 ± 0.49	4.4 ± 0.5
	bioavailability (%)	84 ± 8	78 ± 3	88 ± 13

<sup>a</sup>The vehicle for iv studies was 20% Cavitron, 5% DMSO in PBS.

<sup>b</sup>The vehicle for po studies was 6% Cavitron, 5% DMSO in PBS.

Allometric scaling and in vitro to in vivo extrapolations were used to generate predictions of human PK parameters. These showed a high level of correlation and predicted **6** to have high bioavailability, low clearance, moderate volume and a terminal half-life in the order of 3.3 hours. The average clearance and volume values were then used to reconstruct a mono-exponential predicted human blood concentration time profile, as shown in Figure 5, for once and twice-daily dosing. Doses were scaled and modelled to target maintaining concentrations above the human whole blood  $IC_{90}$  over 24 hours. Inhibitor **6** is predicted to require doses of either 273 daily or 40 mg twice daily to maintain 90% inhibition, with an AUC of 11.7 or 1.7  $\mu\text{g}\cdot\text{h}/\text{mL}$ , respectively. The predicted human PK/PD was modelled using this predicted human PK profile at these doses, along with human whole blood activity, maintaining 90% RIP1 inhibition levels over 24 hours, as shown in the Supporting Information.

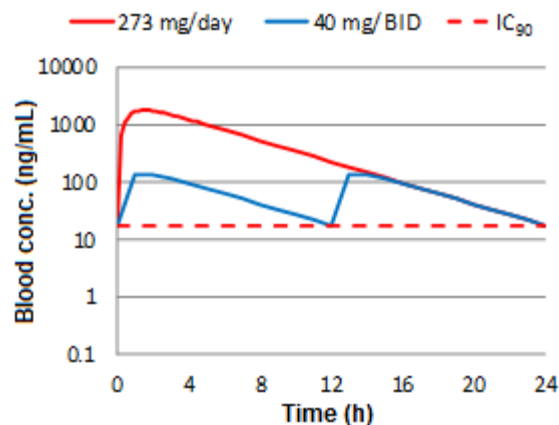


**Figure 5.** Predicted once and twice daily human blood concentration time profile of benzazepinone **6** overlaid with the human whole blood inhibition  $IC_{90}$  concentrations.

## SUMMARY

The emerging biological understanding of the multiple roles of RIP1 kinase has opened up a number of exciting opportunities to investigate this target for drug intervention in a number of diseases. Our recent findings that RIP1 signaling in macrophages regulates immune tolerance in pancreatic cancer and confers resistance to immunotherapy offers a strong rationale that RIP1 kinase inhibition could help address this most significant unmet need in oncology. Benzazepinone **6** was optimized from a DNA-encoded library screen with both high in vitro RIP1 potency and complete kinase selectivity. It has recently initiated phase 1 evaluation in pancreatic cancer patients, the results of which will be reported in future publications.

## ASSOCIATED CONTENT

### Supporting Information

The Supporting Information is available free of charge on the ACS Publications website as a PDF. This contains details on preparation of compounds **2**, **3**, **6-11**, in vitro assays and RIP1 (1-375) preparation. The following data specific to compound **6** is included: mode of inhibition, enzyme kinetics, ortholog inhibition profile, kinase selectivity profile, RIP1 co-crystallization, rat tissue distribution, permeability and P-gp substrate evaluation, hepatocyte turnover and human PK/PD predictions and additional PDOTS evaluation for CD8+ T cells and TNF $\alpha$  expression.

### Accession Codes

Coordinates and structure factors for the cocrystal structure of RIP1 (1-294, C34A, C127A, C233A, C240A) and benzazepinone **6** have been deposited in the Protein Data Bank with the accession number 6RLN.

## AUTHOR INFORMATION

### Corresponding Author

\* E-mail: phaharris100@gmail.com.

### Notes

The authors declare the following competing financial interests: All authors, with the exception of George Miller, Wei Wang, Anirudh Chirala and Dongling Wu, are current employees and stockholders of GlaxoSmithKline.

The human biological samples were sourced ethically, and their research use was in accord with the terms of the informed consents under an IRB/EC approved protocol.

All animal studies were conducted in accordance with the GSK Policy on the Care, Welfare and Treatment of Laboratory Animals and were reviewed the Institutional Animal Care and Use Committee either at GSK or by the ethical review process at the institution where the work was performed.

## ABBREVIATIONS USED

LDH, lactate dehydrogenase; MIP, macrophage inflammatory protein; PDOTS, patient derived organotypic spheroids; RIP, receptor interacting protein; QVD-Oph, (3S)-5-(2,6-difluorophenoxy)-3-[(2S)-3-methyl-1-oxo-2-[(2-quinolinylcarbonyl)amino]butyl]amino]-4-oxopentanoic acid hydrate; SMAC, second mitochondrial-derived activator of caspases; TNF, tumor necrosis factor; zVAD.fmk, carbobenzoxy-valyl-alanyl-aspartyl-[O-methyl]- fluoromethylketone.

## ACKNOWLEDGEMENTS

The authors are indebted to Nicolas Faucher, Nicolas George, Frederic Donche and Alain Daugan from the former GSK group at Les Ulis, France for the design of the in vivo tool inhibitor **5** (GSK'547).

## REFERENCES

- (1) Pasparakis, M.; Vandenabeele, P. Necroptosis and its role in inflammation. *Nature* **2015**, *517*, 311-20.
- (2) Yuan, J.; Amin, P.; Ofengeim, D. Necroptosis and RIPK1-mediated neuroinflammation in CNS diseases. *Nat. Rev. Neurosci.* **2019**, *20*, 19-33.
- (3) Weisel, K.; Scott, N. E.; Tompson, D. J.; Votta, B. J.; Madhavan, S.; Povey, K.; Wolstenholme, A.; Simeoni, M.; Rudo, T.; Richards-Peterson, L.; Sahota, T.; Wang, J. G.; Lich, J.; Finger, J.; Verticelli, A.; Reilly, M.; Gough, P. J.; Harris, P. A.; Bertin, J.; Wang, M. L. Randomized clinical study of safety, pharmacokinetics, and pharmacodynamics of RIPK1 inhibitor GSK2982772 in healthy volunteers. *Pharmacol. Res. Perspect.* **2017**, *5*, e00365.
- (4) Seifert, L.; Miller, G.; Molecular Pathways: The Necrosome - A Target for Cancer Therapy. *Clin. Cancer Res.* **2017**, *23*, 1132-1136.
- (5) Wang, W.; Marinis, J. M.; Beal, A. M.; Savadkar, S.; Wu Y.; Khan, M.; Taunk, P. S.; Wu, N.; Su, W.; Wu, J.; Ahsan, A.; Kurz, E.; Chen, T.; Yaboh, I.; Li, F.; Gutierrez, J.; Diskin, B.; Hundeyin, M.; Reilly, M.; Lich, J. D.; Harris, P. A.; Mahajan, M. K.; Thorpe, J. H.; Nassau, P.; Mosley, J. E.; Leinwand, J.; Kochen, Rossi, J. A.; Mishra, A.; Aykut, B.; Glacken, M.; Ochi, A.; Verma, N.; Kim, J. I.; Vasudevaraja, V.; Adeegbe, D.; Almonte, C.; Bagdatlioglu, E.; Cohen, D. J.; Wong, K. K.; Bertin, J.; Miller, G. RIP1 Kinase Drives Macrophage-Mediated Adaptive Immune Tolerance in Pancreatic Cancer. *Cancer Cell* **2018**, *34*, 757-774.
- (6) Degterev, A.; Hitomi, J.; Germscheid, M.; Ch'en, I. L.; Korkina, O.; Teng, X.; Abbott, D.; Cuny, G. D.; Yuan, C.; Wagner, G.; Hedrick, S. M.; Gerber, S. A.; Lugovskoy, A.; Yuan, J. Identification of RIP1 kinase as a specific cellular target of necrostatins. *Nat. Chem. Biol.* **2008**, *4*, 313-321.
- (7) Xie, T.; Peng, W.; Liu, Y.; Yan, C.; Maki, J.; Degterev, A.; Yuan, J.; Shi Y. Structural basis of RIP1 inhibition by necrostatins. *Structure* **2013**, *21*, 493-499.
- (8) Christofferson, D. E.; Li, Y.; Hitomi, J.; Zhou, W.; Upperman, C.; Zhu, H.; Gerber, S. A.; Gygi, S.; Yuan J. A novel role for RIP1 kinase in mediating TNF $\alpha$  production. *Cell Death Dis.* **2012**, *3*, e320.
- (9) Harris, P. A.; King, B. W.; Bandyopadhyay, D.; Berger, S. B.; Campobasso, N.; Capriotti, C. A.; Cox, J. A.; Dare, L.; Dong, X.; Finger, J. N.; Grady, L. C.; Hoffman, S. J.; Jeong, J. U.; Kang, J.; Kasparcova, V.; Lakdawala, A. S.; Lehr, R.; McNulty, D.E.; Nagilla, R.; Ouellette, M. T.; Pao, C. S.; Rendina, A. R.; Schaeffer, M. C.; Summerfield, J. D.; Swift, B.A.; Totoritis, R.D.; Ward, P.; Zhang, A.; Zhang, D.; Marquis, R. W.; Bertin, J.; Gough, P. J. DNA-Encoded Library Screening Identifies Benzo[b][1,4]oxazepin-4-ones as Highly Potent and Monoselective Receptor Interacting Protein 1 Kinase Inhibitors. *J. Med. Chem.* **2016**, *59*, 2163-2178.
- (10) Harris, P. A.; Berger, S. B.; Jeong, J. U.; Nagilla, R.; Bandyopadhyay, D.; Campobasso, N.; Capriotti, C. A.; Cox, J. A.; Dare, L.; Dong, X.; Eidam, P. M.; Finger, J. N.; Hoffman, S. J.; Kang, J.; Kasparcova, V.; King, B. W.; Lehr, R.; Lan, Y.; Leister, L. K.; Lich, J. D.; MacDonald, T. T.; Miller, N. A.; Ouellette, M. T.; Pao, C. S.; Rahman, A.; Reilly, M. A.; Rendina, A. R.; Rivera, E. J.; Schaeffer, M. C.; Sehon, C. A.; Singhaus, R. R.; Sun, H. H.; Swift, B. A.; Totoritis, R. D.; Vossenkämper, A.; Ward, P.; Wisnoski, D. D.; Zhang, D.; Marquis, R. W.; Gough P. J.; Bertin, J. Discovery of a First-in-Class Receptor Interacting Protein 1 (RIP1) Kinase Specific Clinical Candidate (GSK2982772) for the Treatment of Inflammatory Diseases. *J. Med. Chem.* **2017**, *60*, 1247-1261.
- (11) Yoshikawa, M.; Saitoh, M.; Katoh, T.; Seki, T.; Bigi, S. V.; Shimizu, Y.; Ishii, T.; Okai, T.; Kuno, M.; Hattori, H.; Watanabe, E.; Saikatendu, K. S.; Zou, H.; Nakakariya, M.; Tatamiya, T.; Nakada, Y.; Yogo, T. Discovery of 7-Oxo-2,4,5,7-tetrahydro-6 H-pyrazolo[3,4- c]pyridine Derivatives as Potent, Orally Available, and Brain-Penetrating Receptor Interacting Protein 1 (RIP1) Kinase Inhibitors: Analysis of Structure-Kinetic Relationships. *J. Med. Chem.* **2018**, *61*, 2384-2409.
- (12) Jenkins, R. W.; Aref, A. R.; Lizotte, P. H.; Ivanova, E.; Stinson, S.; Zhou, C. W.; Bowden, M.; Deng, J.; Liu, H.; Miao, D.; He, M. X.; Walker, W.; Zhang, G.; Tian, T.; Cheng, C.; Wei, Z.; Palakurthi, S.; Bittinger, M.; Vitzthum, H.; Kim, J. W.; Merlino, A.; Quinn, M.; Venkataramani, C.; Kaplan, J. A.; Portell, A.; Gokhale, P. C.; Phillips, B.; Smart, A.; Rotem, A.; Jones, R. E.; Keogh, L.; Anguiano, M.; Stapleton, L.; Jia, Z.; Barzily-Rokni, M.; Cañadas, I.; Thai, T. C.; Hammond, M. R.; Vlahos, R.; Wang, E. S.; Zhang, H.; Li, S.; Hanna, G. J.; Huang, W.; Hoang, M. P.; Piris, A.; Eliane, J. P.; Stemmer-Rachamimov, A. O.; Cameron, L.; Su, M. J.; Shah, P.; Izar, B.; Thakuria, M.; LeBoeuf, N. R.; Rabinowits, G.; Gunda, V.; Parangi, S.; Cleary, J. M.; Miller, B. C.; Kitajima, S.; Thummalapalli, R.; Miao, B.; Barbie, T. U.; Sivathanu, V.; Wong, J.; Richards, W. G.; Bueno, R.; Yoon, C. H.; Miret, J.; Herlyn, M.; Garraway, L. A.; Van Allen, E. M.; Freeman, G. J.; Kirschmeier, P. T.; Lorch, J. H.; Ott, P. A.; Hodi, F. S.; Flaherty, K. T.; Kamm, R. D.; Boland, G. M.; Wong, K. K.; Dornan, D.; Paweletz, C. P.; Barbie DA. Ex Vivo Profiling of PD-1 Blockade Using Organotypic Tumour Spheroids. *Cancer Discov.* **2018**, *8*, 196-215.
- (13) Fridman, W. H.; Zitvogel, L.; Sautes-Fridman, C.; Kroemer G. The immune contexture in cancer prognosis and treatment. *Nat. Rev. Clin. Oncol.* **2017**, *14*, 717-734.

## Table of Contents/Abstract Graphic

